Supporting Information

Reconfiguration of Band-edge States via Intermolecular Packing in Organic Semiconductor-Incorporated Perovskites

Jia Xu,[a] Zhun Liu,[a] Xieli Wei,[a] Junqiang Lu,[a] Qifeng Liang[a] and Jijun Zhao[b]*

[a] Faculty of Department of Physics, Shaoxing University, Shaoxing 312000, China

[b] 1. Guangdong Basic Research Center of Excellence for Structure and Fundamental Interactions of Matter, Guangdong Provincial Key Laboratory of Quantum Engineering and Quantum Materials, School of Physics, South China Normal University, Guangzhou 510006, China. 2. Guangdong-Hong Kong Joint Laboratory of Quantum Matter, Frontier Research Institute for Physics, South China Normal University, Guangzhou 510006, China

[*] Corresponding Author. Email: liu6zhun@163.com

Calculation of the formation energy (ΔH_{form})

Formation energy, a crucial factor of the chemical and thermodynamic stability of materials, has been widely applied.[1] The negative formation enthalpy indicates that these 2D perovskites can be spontaneously synthesized under specific experimental conditions, as evaluated by the average formation energy on per chemical unit:[2]

$$\Delta H_{form} = \frac{E_{(AEmT)Cs_{n-1}Pb_nI_{3n+1}} - E_{(AEmT)I_2} - nE_{PbI_2} - (n-1)E_{CsI}}{n}$$

where $E_{(AEmT)Cs_{n-1}Pb_nI_{3n+1}}$, E_{PbI_2} and E_{CsI} are the energies of bulk (AEmT)$Cs_{n-1}Pb_nI_{3n+1}$, PbI_2 and CsI, and $E_{(AEmT)I_2}$ is the energy of gas phase (AEmT)I_2. When calculating the energy of gas phase molecules, it is necessary to establish large periodic cells to avoid interplays between neighboring molecules.

Work function (ϕ)

The work function (ϕ) represents the minimum energy required for an electron to escape from its surface to the vacuum, significantly influencing the quantum efficiency (QE) of a photocathode.[3,4] To compare the changes in energy level positions, we aligned the work function of OSiPs relative to the vacuum level to determine ionization energy and the overall band edge positions.[5] The calculated ϕ can be described as

$$\phi = E_{vacuum} - E_{Fermi}$$

where E_{vacuum} and E_{Fermi} are the vacuum energy level and Fermi energy of the material, respectively.[6]

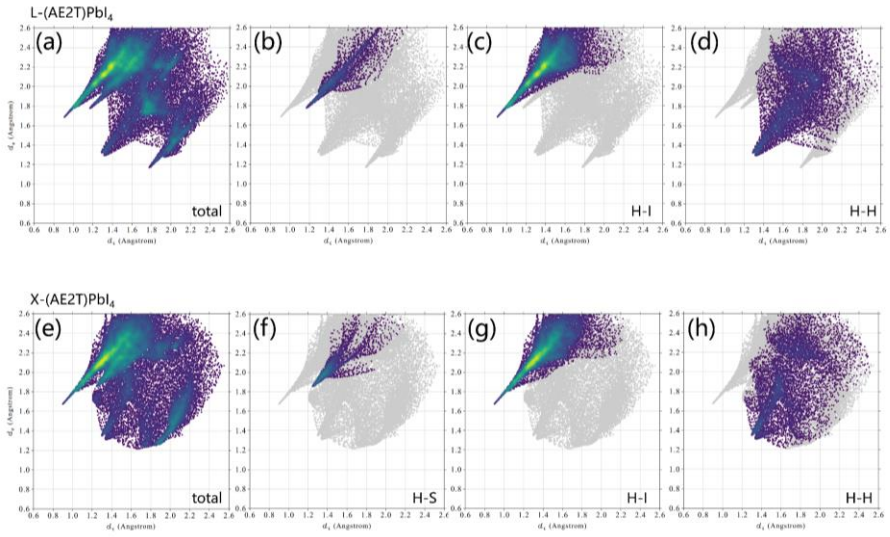

Fig. S1. Fingerprint plots with the density distribution of each vertex on the Hirshfeld surface of L-(AE2T)PbI_4 and X-(AE2T)PbI_4.

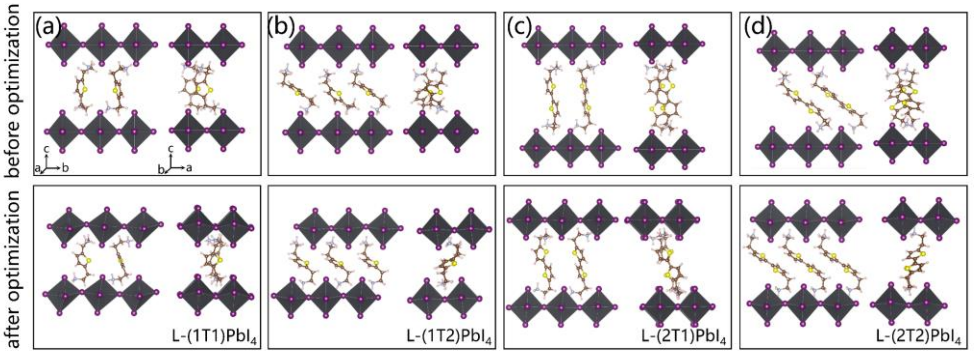

Fig. S2. Front and side views of L-parallel-type OSiPs in AE1T (a) L-(1T1)PbI_4, (b) L-(1T2)PbI_4, and AE2T series (c) L-(2T1)PbI_4, (d) L-(2T2)PbI_4 before and after geometry optimization, selected for stacking arrangements.

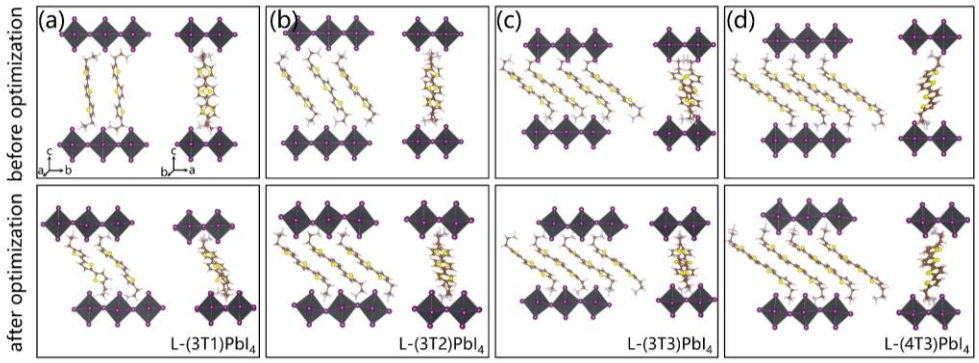

Fig. S3. Front and side views of L-parallel-type OSiPs in AE3T series (a) L-(3T1)PbI_4, (b) L-(3T2)PbI_4, (c) L-(3T3)PbI_4, and a supplementary (d) L-(4T3)PbI_4 before and after geometry optimization, selected for stacking arrangements.

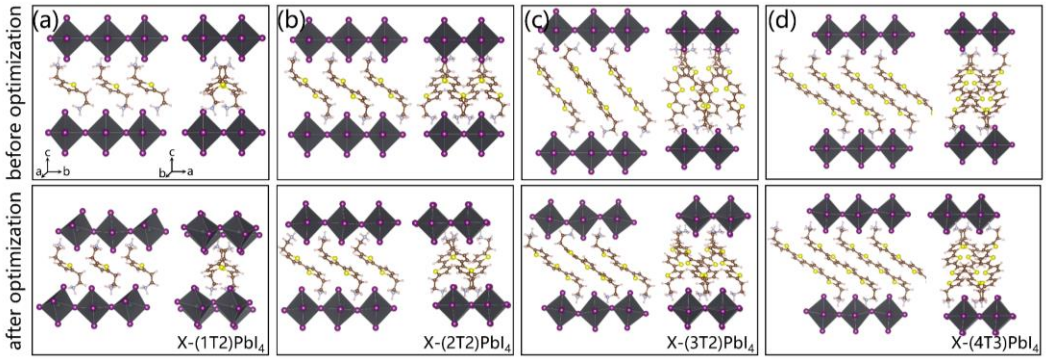

Fig. S4. Front and side views of X-herringbone-type OSiPs (a) X-(1T2)PbI_4, (b) X-(2T2)PbI_4, (c) X-(3T2)PbI_4, and a supplementary (d) L-(4T3)PbI_4 before and after geometry optimization.

The thiophene rings within each AEmT (m=1-3) moiety are coplanar and adopt the "all-anti" configuration. To be consistent with the quaterthiophene molecule in experiments, AE4T adopts a "syn-anti-syn" configuration.[7] Additionally, to ensure compatibility with the structures of single-crystal X-ray analysis, L-(2T2)PbI_4, X-

(2T2)PbI_4, L-(4T3)PbI_4, and X-(4T3)PbI_4 were optimized based on their experimental structure.[7,8] Since the stacking arrangements of AE4T series OSiPs have been firmly established, only their orientations were adjusted as a supplementary investigation, as depicted in **Fig. S3(d)** and **S4(d)**. For the remaining series of polymorphs, for which crystal structures have not yet been experimentally obtained, the unit cells were approximated from similar thiophene derivatives by adjusting the organic cations and inserting or deleting the additional thiophene molecules.[9] "**L**" or "**X**" refers to the parallel or herringbone arrangement of molecules, respectively, which dictated the stacking arrangement of the organic ligands when their orientation along the b-axis differed. Moreover, the flexible ethylammonium tethering groups linking the perovskite layers through hydrogen bonding allowed for the possibility of these two types of polymorphs. Consequently, these OSiPs could be synthesized under controllable conditions.

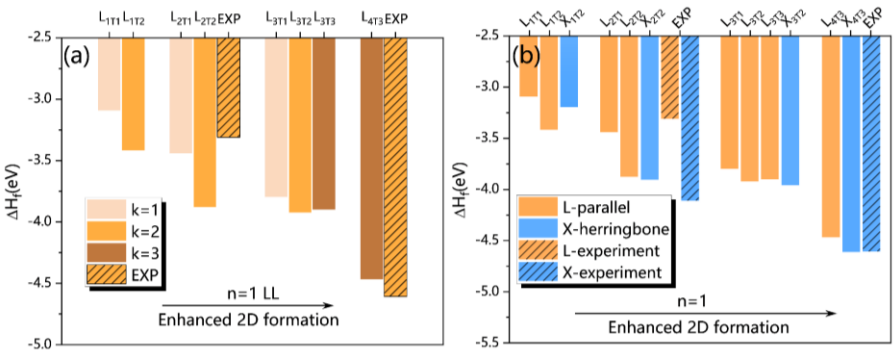

Fig. S5. The formation enthalpies of OSiPs in (a) 8 distinct stacking arrangements of L-parallel polymorph structures and partially experimentally resolved structures (blocks with diagonal lines) at n=1. (b) all the candidate OSiPs and partially experimentally resolved structures (blocks with diagonal lines) at n=1. Experimental OSiPs (x-ray diffraction) come from recently reported (AE2T)PbI_4[8] and (AE4T)PbI_4.[7,10] We identified the L-parallel stacking arrangement of OSiPs and selected the candidates with the lowest formation enthalpy, then altered their orientation to form the X-herringbone-type OSiP.

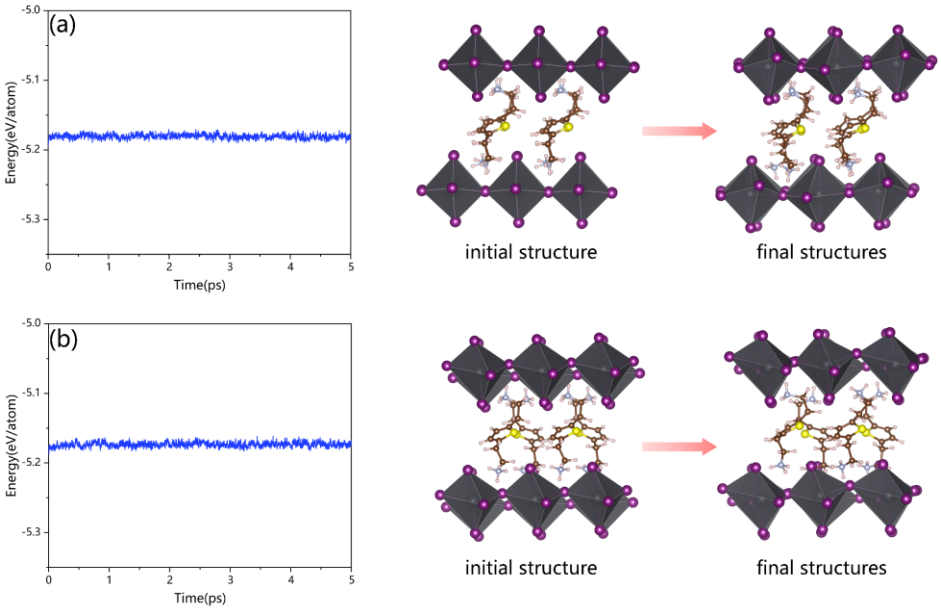

Fig. S6. The energy fluctuation and structural variation of (a)L-(1T2)PbI_4 (n=1), (b)X-(1T2)PbI_4 (n=1) during Ab initio molecular dynamics (AIMD) simulation of 5 ps under 300 K.

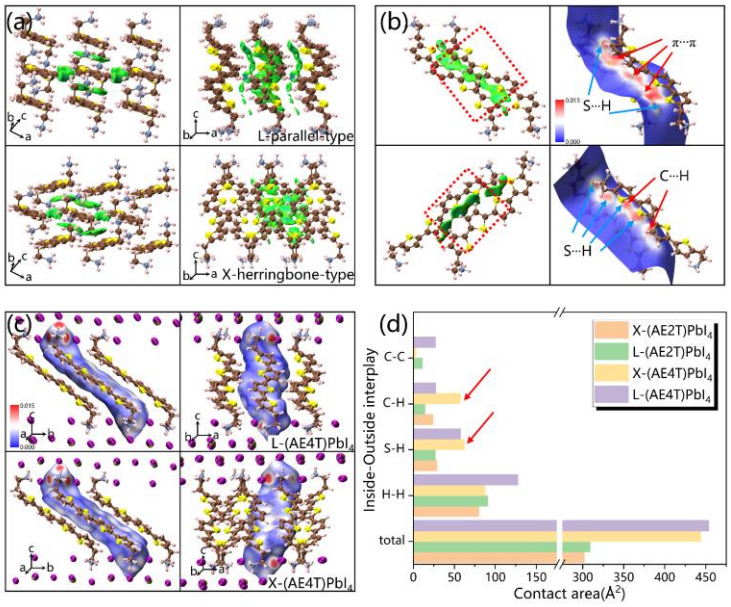

Fig. S7. Analysis of intermolecular interactions of the optimized L-(AE4T)PbI_4 and X-(AE4T)PbI_4. (a) Green IGM isosurface maps (isosurface = 0.005 a.u.) between the central molecule and its eight neighboring molecules, the size of IGM isosurface maps represents the strength of intermolecular interactions. (b) Single green IGM isosurface maps (isosurface = 0.005 a.u.) and 2D Hirshfeld surface analyses for two independent adjacent face/edge-to-face molecules. (c) 3D Hirshfeld surface analysis for central AE4T within OSiPs colored by electron density. (d) The enumerated main contact areas between inside-outside interplays in L-(AE2T)PbI_4, X-(AE2T)PbI_4, L-(AE4T)PbI_4, and X-(AE4T)PbI_4, respectively.

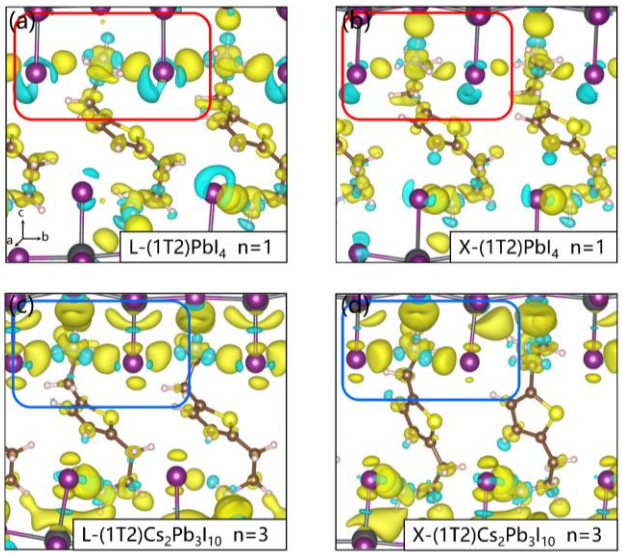

Fig. S8. Charge density differences of AE1T series OSiPs calculated by the formula, $\Delta\rho = \rho_{total} - \rho_{organic\ ligands} - \rho_{inorganic\ layers}$, where ρ is the total charge density. (a)L-(1T2)PbI_4 (n=1), (b)X-(1T2)PbI_4 (n=1), (c)L-(1T2)$Cs_2Pb_3I_{10}$ (n=3), and (d)X-(1T2)$Cs_2Pb_3I_{10}$ (n=3). The yellow part indicates charge accumulation, while the cyan part represents charge depletion.

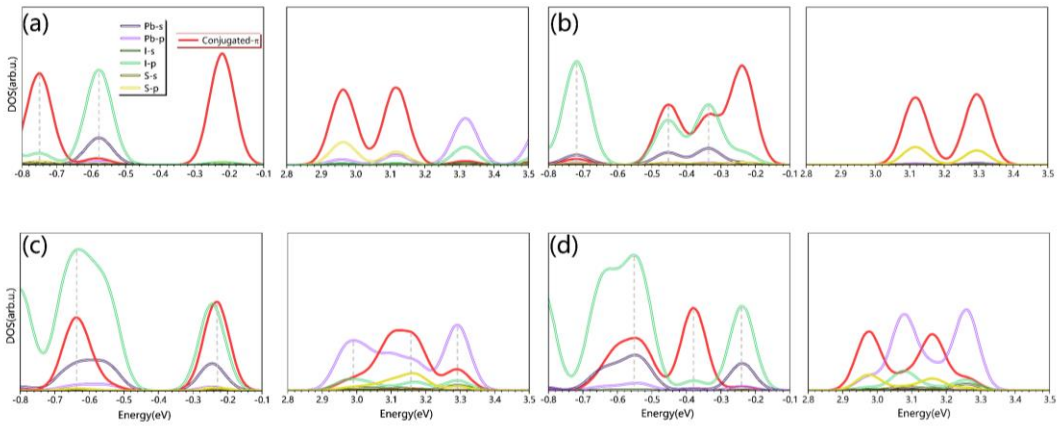

Fig. S9. Projected density of state (PDOS) of *s*, *p* orbitals of Pb, I, S and the *p* orbital of C in conjugated π bonds in AE2T series of OSiPs. (a)L-(2T2)PbI_4, (b)X-(2T2)PbI_4, (c)L-(2T2)$Cs_2Pb_3I_{10}$, and (d)X-(2T2)$Cs_2Pb_3I_{10}$.

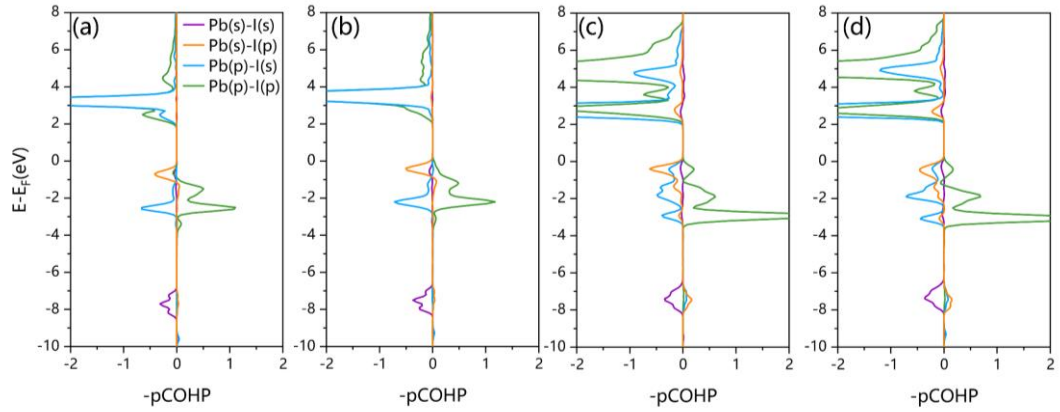

Fig. S10. Orbital-resolved crystal orbital Hamilton populations (COHP) analysis for Pb-I interplays of (a)L-(2T2)PbI_4, (b)X-(2T2)PbI_4, (c)L-(2T2)$Cs_2Pb_3I_{10}$, and (d)X-(2T2)$Cs_2Pb_3I_{10}$. The positive and negative sign indicates the bonding and anti-bonding characters, respectively.

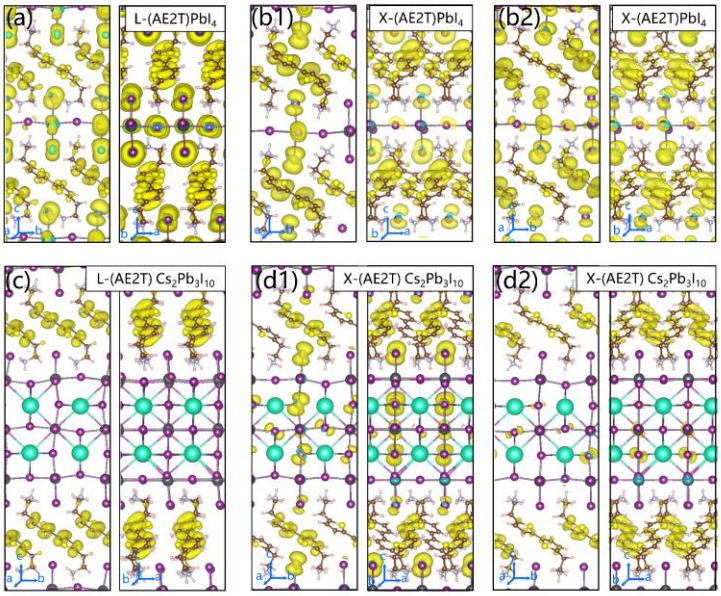

Fig. S11. Calculated frontier molecular orbital profiles of (a)L-(2T2)PbI_4 (HOMO), (b1)(b2)X-(2T2)PbI_4 (HOMO and HOMO-1), (c)L-(2T2)$Cs_2Pb_3I_{10}$ (HOMO), and (d1)(d2)X-(2T2)$Cs_2Pb_3I_{10}$ (HOMO and HOMO-1).

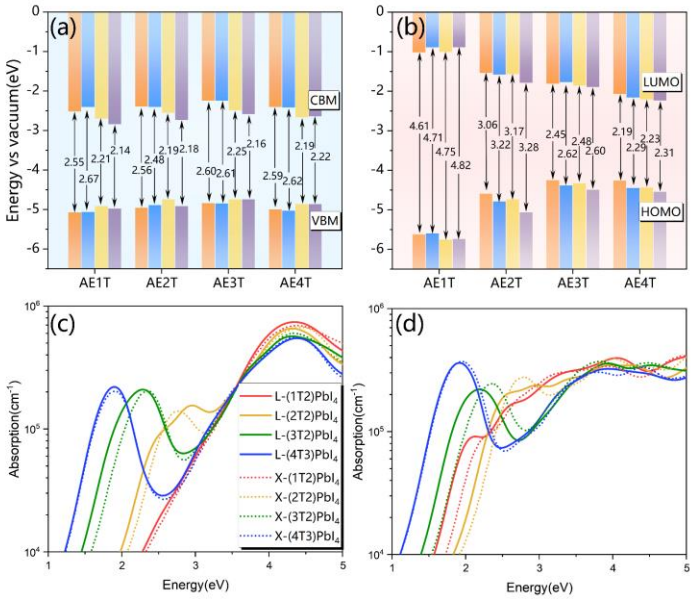

Fig. S12. The frontier bands with respect to the vacuum level of (a)inorganic (light blue background) and (b)organic (light pink background) layers within OSiPs, respectively. Optical absorption spectra of (c)out-of-plane and (d)in-plane for monolayer OSiPs, respectively.

Table S1. Calculated bandgaps

	HSE+SOC	SOC	PBE	HSE+SOC	SOC	PBE
	n=1	n=1	n=1	n=3	n=3	n=3
L-(1T2)PbI_4	2.6653	1.1186	1.8391	2.3439	0.8258	1.6478
X-(1T2)PbI_4	2.7930	1.2427	1.9239	2.2432	0.7844	1.6035
L-(2T2)PbI_4	2.3326	1.1553	1.7323	2.3010	0.8095	1.6410
X-(2T2)PbI_4	2.4929	1.1126	1.7965	2.3234	0.7701	1.5870
L-(3T2)PbI_4	2.1404	0.9859	1.4186	1.9838	0.8471	1.4089
X-(3T2)PbI_4	2.2560	1.0005	1.4528	2.0492	0.7869	1.5547
L-(4T3)PbI_4	1.9917	0.9931	1.5011	1.8920	0.7576	1.4738
X-(4T3)PbI_4	2.1514	1.0655	1.6204	2.0326	0.7871	1.6218

Table S2. Calculated effective masses for 6 selected OSiPs with SOC. The higher hole effective masses mainly contributed from the small band dispersion of molecular components.

	Effective mass at band edges	
	m_e*	m_h*
L-(1T2)PbI_4	0.303	0.257
L-(2T2)PbI_4	0.293	5.140
L-(3T2)PbI_4	0.200	5.604
X-(1T2)PbI_4	0.260	0.256
X-(2T2)PbI_4	0.278	0.528
X-(3T2)PbI_4	0.144	5.734

REFERENCES

1 W.-J. Yin, Y. Yan and S.-H. Wei, *J. Phys. Chem. Lett.*, 2014, **5**, 3625–3631.

2 L. N. Quan, M. Yuan, R. Comin, O. Voznyy, E. M. Beauregard, S. Hoogland, A. Buin, A. R. Kirmani, K. Zhao, A. Amassian, D. H. Kim and E. H. Sargent, *J. Am. Chem. Soc.*, 2016, **138**, 2649–2655.

3 R. Xiang and J. Teichert, *Phys. Procedia*, 2015, **77**, 58–65.

4 R. Jacobs, J. Booske and D. Morgan, *Adv. Funct. Mater.*, 2016, **26**, 5471–5482.

5 S. G. Lewis, D. Ghosh, K. L. Jensen, D. Finkenstadt, A. Shabaev, S. G. Lambrakos, F. Liu, W. Nie, J.-C. Blancon, L. Zhou, J. J. Crochet, N. Moody, A. D. Mohite, S. Tretiak and A. J. Neukirch, *J. Phys. Chem. Lett.*, 2021, **12**, 6269–6276.

6 C. Kittel, *Introduction to solid state physics*, Wiley, Hoboken, NJ, 8th ed., 2005.

7 D. B. Mitzi, K. Chondroudis and C. R. Kagan, *Inorg. Chem.*, 1999, **38**, 6246–6256.

8 M. K. Jana, C. Liu, S. Lidin, D. J. Dirkes, W. You, V. Blum and D. B. Mitzi, *Chem. Mater.*, 2019, **31**, 8523–8532.

9 J. Y. Park, R. Song, J. Liang, L. Jin, K. Wang, S. Li, E. Shi, Y. Gao, M. Zeller, S. J. Teat, P. Guo, L. Huang, Y. S. Zhao, V. Blum and L. Dou, *Nat. Chem.*, , DOI:10.1038/s41557-023-01311-0.

10 C. Liu, W. Huhn, K.-Z. Du, A. Vazquez-Mayagoitia, D. Dirkes, W. You, Y. Kanai, D. B. Mitzi and V. Blum, *Phys. Rev. Lett.*, 2018, **121**, 146401.